

## Brillouin light scattering study of magnetic-element normal modes in a square artificial spin ice geometry

This content has been downloaded from IOPscience. Please scroll down to see the full text.

2017 J. Phys. D: Appl. Phys. 50 015003

(<http://iopscience.iop.org/0022-3727/50/1/015003>)

View [the table of contents for this issue](#), or go to the [journal homepage](#) for more

Download details:

IP Address: 129.11.23.120

This content was downloaded on 26/01/2017 at 11:00

Please note that [terms and conditions apply](#).

You may also be interested in:

[Brillouin light scattering studies of 2D magnonic crystals](#)

S Tacchi, G Gubbiotti, M Madami et al.

[Brillouin light scattering studies of planar metallic magnonic crystals](#)

G Gubbiotti, S Tacchi, M Madami et al.

[Magnetic properties of layered nanostructures](#)

Giovanni Carlotti and Gianluca Gubbiotti

[From micro- to nanomagnetic dots: evolution of the eigenmode spectrum on reducing the lateral size](#)

G Carlotti, G Gubbiotti, M Madami et al.

[Discrete modes of a ferromagnetic stripe dipolarly coupled to a ferromagnetic film: a Brillouin light scattering study](#)

G Gubbiotti, S Tacchi, G Carlotti et al.

[Field dependence of the magnetic eigenmode frequencies in layered nanowires with ferromagnetic and antiferromagnetic ground states: experimental and theoretical study](#)

G Gubbiotti, H T Nguyen, R Hiramatsu et al.

[Review and prospects of magnonic crystals and devices with reprogrammable band structure](#)

M Krawczyk and D Grundler

[Brillouin light scattering study of  \$\text{Co}\_2\text{Cr}\_{0.6}\text{Fe}\_{0.4}\text{Al}\$  and  \$\text{Co}\_2\text{FeAl}\$  Heusler compounds](#)

O Gaier, J Hamrle, S Trudel et al.

[Collective spin waves on a nanowire array with step-modulated thickness](#)

G Gubbiotti, M Kostylev, S Tacchi et al.

# Brillouin light scattering study of magnetic-element normal modes in a square artificial spin ice geometry

Y Li<sup>1</sup>, G Gubbiotti<sup>2</sup>, F Casoli<sup>3</sup>, F J T Gonçalves<sup>1</sup>, S A Morley<sup>4</sup>,  
M C Rosamond<sup>5</sup>, E H Linfield<sup>5</sup>, C H Marrows<sup>4</sup>, S McVitie<sup>1</sup> and R L Stamps<sup>1</sup>

<sup>1</sup> SUPA School of Physics and Astronomy, University of Glasgow, Glasgow G12 8QQ, UK

<sup>2</sup> Istituto Officina dei Materiali del Consiglio Nazionale delle Ricerche (IOM-CNR), Sede di Perugia, c/o Dipartimento di Fisica e Geologia, Via A. Pascoli, I-06123 Perugia, Italy

<sup>3</sup> IMEM-CNR, I-43124 Parma, Italy

<sup>4</sup> School of Physics and Astronomy, University of Leeds, Leeds LS2 9JT, UK

<sup>5</sup> School of Electronic and Electrical Engineering, University of Leeds, Leeds LS2 9JT, UK

E-mail: [robert.stamps@glasgow.ac.uk](mailto:robert.stamps@glasgow.ac.uk)

Received 30 May 2016, revised 26 October 2016

Accepted for publication 31 October 2016

Published 23 November 2016



## Abstract

We report the results, from experimental and micromagnetic studies, of the magnetic normal modes in artificial square spin ice systems consisting of ferromagnetic-monodomain islands. Spin-wave properties are measured by Brillouin light scattering. The mode spectra contain several branches whose frequencies are sensitive to the magnitude and in-plane orientation of an applied magnetic field. We also identify soft modes that exhibit different behaviours depending on the direction of the applied magnetic field. The obtained results are well described with micromagnetic simulations of independent magnetic elements arranged along two sublattices.

Keywords: hysteresis loop, spin wave, magnetic normal mode, artificial spin ice


(Some figures may appear in colour only in the online journal)

## 1. Introduction

Artificial spin ice (ASI) is a class of magnetic materials created by patterning single domain ferromagnetic islands in such a way as to introduce some degree of frustration through interactions determined geometrical constraints [1]. Square ASI is one of the first and best studied ice geometries [2, 3], along with the fully frustrated kagome lattices [4]. A variety of other structures have also been studied, including Penrose [5] and Shatki lattices [6, 7] as well as suggestions for many others [11, 12]. The magnetic elements are typically fashioned as elongated islands with nano-scale dimensions in order to ensure that their magnetic state is single domain with a large uniaxial shape anisotropy so as to approximate a rigid block

spin [13–15]. An appealing aspect of the ASI is the ability to modify macroscopic magnetic properties through design of the ASI geometry and generate new functionality [5, 7, 16]. There have been a few works published that begin to explore possibilities for reconfigurable microwave devices using an artificial spin ice platform. In some cases evidence for interelement interactions is present [8], but not in others [9, 10]. In our study we examine a case in which interelement interactions are negligible in order to highlight instead only configurational aspects which, even on their own, turn out to be complex.

The magnetically soft transition metals commonly used to fabricate ASI exhibit high frequency electromagnetic resonances in the GHz range. The resonances correspond to band center spin waves, which are the fundamental magnetic excitations of a magnetic material. Resonances of spin waves can be studied at long wavelengths using Brillouin light scattering (BLS). This technique has been used to obtain experimental

 Original content from this work may be used under the terms of the [Creative Commons Attribution 3.0 licence](https://creativecommons.org/licenses/by/3.0/). Any further distribution of this work must maintain attribution to the author(s) and the title of the work, journal citation and DOI.

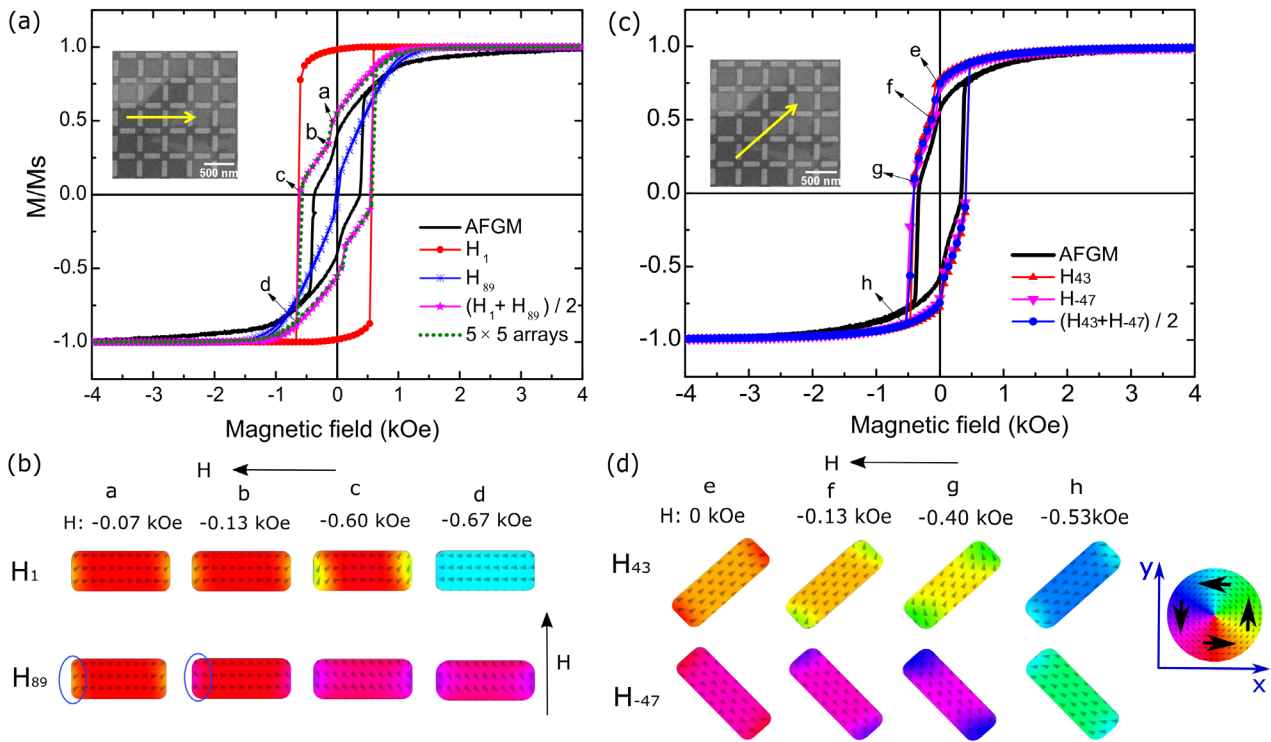


**Figure 1.** Hysteresis loops of the AGFM measurements and numerical simulation at (a)  $0^\circ$  and (c)  $45^\circ$  applied field with respect to the ASI lattices, in which insets are SEM images showing the geometry of ASI lattices and the orientation of external field (yellow arrows). Ground-state magnetization configurations at the (b) parallel and (d) diagonal field, and color code disk represents the direction of magnetization.

values for a number of magnetic parameters: magnetic anisotropy [17, 18], gyromagnetic ratio [19] and exchange constants [20].

The mode structure of spin waves in individual elements is well understood [24]. Spin-wave modes observed in micron and submicron sized magnetic elements are confined modes with stationary character [21]. For the geometry of element studied here, the detected modes have mainly magnetostatic character. Most importantly for this work, modes exist which are localised to edges of magnetic elements. These modes have dipolar stray fields [24] which extend away from the material, although they decay away from the magnetic material into the surrounding medium. In addition, since the elements are in a single-domain state, there is a nonuniform distribution of demagnetising fields in the elements, which is most pronounced near the edges and corners. These can lead to some curling of the magnetisation within an exchange length of the edges, and mostly serves to affect the frequency of a mode localised to the edge. The frequency of this edge mode is lower than the geometrical resonance of the elements studied here.

Previous investigations of the spin-wave modes in rectangular islands elements have been performed for arrays where all islands are oriented in the same direction [22, 23]. In our array we are able to create the complex arrangements of magnetic elements, and gain some information about their configurations by scattering from microwave excitations. Our general findings are that all features observed in BLS experiment can be described by the modes associated with individual elements in the square ASI. The elements lie along the sides of squares, as shown in the inset of figure 1(a), and the

frequencies of modes depend upon whether the magnetization of individual elements are aligned by the applied field along easy or hard directions of the elements. We have found that, depending on the direction of the applied field, the frequency evolution exhibits complex and peculiar features. Mode softening and ‘bell’ shape in frequency versus field have been observed in coincidence with the magnetization reversal for  $H$  applied along the ASI edge. For  $H$  at ( $45^\circ$ ) with respect the ASI edge, the frequency monotonically evolves as a function of the applied field. We use micromagnetic simulation to identify the excitations measured in the independent elements.

The paper is organised as follows. The experimental results from alternating gradient force magnetometry and the analysis in terms of single element reversal for different field orientations are presented in the next section. Results from BLS with a micromagnetic analysis of mode frequencies and profiles are discussed in the third section. The conclusions are presented in the final section.

## 2. Sample preparation and magnetic hysteresis

Square spin ice lattices ( $\text{Ni}_{80}\text{Fe}_{20}$ ) were patterned on oxidised silicon substrate by electron beam lithography. A mask with the square ASI array shape was written and developed by the 100kV electron beam on the positive resist. The NiFe was electron-beam evaporated and then the unpatterned NiFe film and mask were removed. The ASI studied has the island of  $240 \text{ nm} \times 80 \text{ nm}$  in size and 10 nm thickness, with a 450 nm lattice constant. Correspondingly, the corner-to-corner

distance between the first nearest neighbouring islands is approximately 92 nm.

Hysteresis loops were measured using alternating gradient force magnetometry (AGFM). The magnetic field was applied along directions that make angles of  $0^\circ$  and  $45^\circ$  with the axes of the ASI square lattices, with values between +15 kOe to -15 kOe. The experimental hysteresis loops are shown by the black solid lines in panels (a) and (c) of figure 1. In figure 1(a), the field is aligned along a horizontal edge of the array ( $0^\circ$ ), and in figure 1(c) the field is aligned along a diagonal ( $45^\circ$ ) of the square ASI lattices.

So as to identify features arising from element interactions, the results from micromagnetic simulations of hysteresis for single elements are also shown in figures 1(b) and (d) for comparison. The simulations were performed using MuMax3 [25], and were done for isolated elements representing separately the horizontal and vertical islands constituting the array. The saturation magnetization  $M_s$  and exchange constant  $A$  of Permalloy material were taken as  $800 \text{ kA m}^{-1}$  and  $10^{-11} \text{ J m}^{-1}$  [26], respectively. A grid with 10 nm thickness and  $2.4 \text{ nm} \times 2.4 \text{ nm}$  lateral size of cell was used, which is less than the exchange length  $l = \sqrt{2A/\mu_0 M_s^2}$  [27], here  $l = 5 \text{ nm}$ . Hysteresis loops of elements were calculated for the field aligned parallel to: the horizontal axis  $H_1$ ; the vertical axis  $H_{89}$ ; and the diagonal axes  $H_{43}$  and  $H_{-47}$ . These configurations are sketched in figures 1(b) and (d) for clarity. It should be noted that the magnetic field was slightly misaligned from the horizontal by  $1^\circ$  and diagonal by  $2^\circ$  in order to avoid possible artefacts associated with unstable states that can appear with the field aligned in highly symmetric configurations. Therefore, in the simulation the ASI elements with respect to the orientation of field are denoted as  $H_1$ ,  $H_{89}$ ,  $H_{43}$  and  $H_{-47}$ . The hysteresis loops, in which the magnetization is the mean value over the whole grid, are shown in figures 1(a) and (c) by coloured symbols, along with their averages.

We first consider the hysteresis with the field applied along a horizontal edge direction shown in figure 1(a). Going from positive field to negative, we see that general features of the measured hysteresis are visible in the averaged simulation results (shown by the star symbol curve). There is a change in slope beginning at 1 kOe, followed by sharp drops at 0 (marked 'a') and 0.7 kOe (marked 'c'). The drop at 'a' corresponds to rotation of the hard axis elements ( $H_{89}$ ) ends (shown by the blue circles), and the plummet at 'c' corresponds to the reversal of the magnetic moment in the easy axis island ( $H_1$ ).

The reversal of magnetization within individual elements is predicted to occur differently for the horizontal ( $H_1$ ) and vertical elements ( $H_{89}$ ) in the ASI lattices. Example spin configurations are shown in figure 1(b) where the magnetization direction is mapped for  $H_1$  and  $H_{89}$  elements using colour coding. The configurations are shown for positions on the hysteresis loops 'a', 'b', 'c' and 'd'. In general, these two groups of the elements reverse through an 'S' magnetization configuration with an unsaturated field.

To examine possible interaction effects, we also show simulated hysteresis for a five by five array of elements with a dotted curve. The simulated array follows the average curve

exactly, suggesting that finite size effects that might be associated with reversal of edge elements in the array do not seem to play a large effect. We also note that the measured curve shows a decrease between 3 kOe and 1 kOe that is not visible in the simulations. This may be associated with imperfections of the elements. There is also disagreement between the coercive fields determined by measurement and simulation. This may result in part from nucleation sites generated by irregularly shaped islands as opposed to the ideally identical shape of ASI island in the micromagnetic calculation [28]. Another possibility is that the temperature in simulation is absolute zero degree, while measurement are performed at room temperature.

The analysis of the hysteresis for the field applied along a diagonal orientation is shown in figures 1(c) and (d). Agreement is much closer between measured and simulated curves in this case. The two elements reverse in the same manner, as one would expect, and there is good agreement at coercive fields. The measured hysteresis is still reduced from the calculated loop at high fields, probably for the same reasons as discussed above, namely actual versus ideal sample shapes.

One question we could ask is if we can identify features from hysteresis alone that indicate effects associated with interactions between elements. For application of the field along a diagonal direction it appears possible to describe the magnetization processes observed for the square ASI in terms of reversals of individual non-interacting elements. The situation is different for hysteresis with the field aligned along a horizontal edge. The general features observed in the hysteresis are qualitatively similar to what one would predict from an ensemble of non-interacting elements, but there are significant quantitative differences apparent in the unsaturated region. It is in this field region precisely that we would expect effects of inter-element interactions to be most apparent as they modify locally the fields driving element reversals. We turn next to measurements of spin waves which are able to provide additional information about local effective fields.

### 3. Brillouin light scattering and magnetic normal mode properties

Brillouin light scattering technique is used to measure the spectrum of magnetic excitations in ASI array. This technique is sensitive to low frequency modes, and can detect excitations that may not be visible using ferromagnetic resonance spectrum. BLS spectra of the thermal magnetic excitation were collected at room temperature in the backscattering geometry by using a (3 + 3)-pass tandem Fabry–Perot interferometer. A monochromatic laser ( $\lambda = 532 \text{ nm}$ ) with 200 mW power was focused into a spot with  $30 \mu\text{m}$  diameter. This means that in the BLS spectra several hundreds of ASI islands are illuminated and therefore the information obtained is averaged over a large number of the elements [29].

In order to investigate the spin-wave properties of such ASI array we performed two types of BLS measurement to probe wavevector and field dependences. Firstly, to measure the

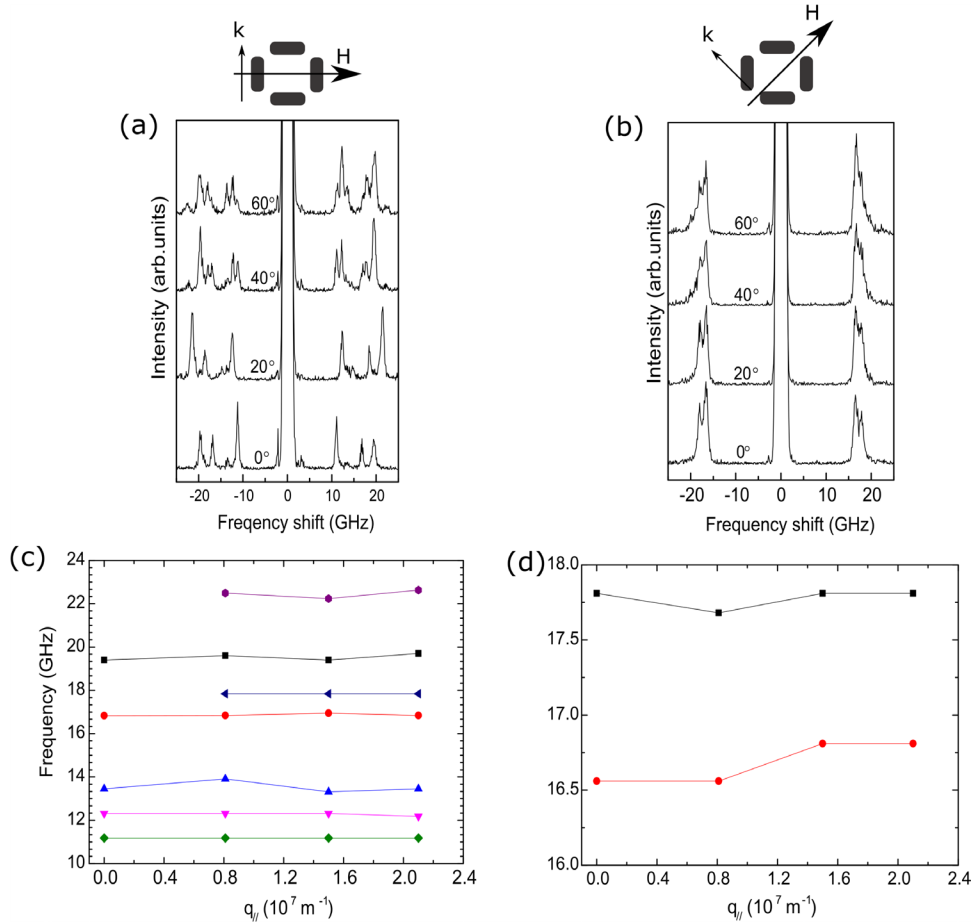


**Figure 2.** Sequence of BLS spectra measured at different incidence angles  $\theta$  with the external field of 3 kOe at (a)  $0^\circ$  and (b)  $45^\circ$  upon the ASI lattices. The wavevector of the incident light is perpendicular to the field orientation in Damon–Eshbach configuration. Spin-wave frequency on the Stokes side as a function of the in-plane wavenumber at a 3 kOe (c) parallel field and (d) diagonal field. Dots are experimental data and lines are guides for the eyes.

frequency dependence on the wavevector ( $q_{\parallel}$ ) the applied field was fixed at 3 kOe along directions at  $0^\circ$  and  $45^\circ$  with respect to the ASI lattices. The angle of incident light  $\theta$  upon the sample varied from  $0^\circ$  to  $60^\circ$  corresponding to in-plane wavenumber  $q_{\parallel}$  from 0 to  $2 \times 10^7 \text{ m}^{-1}$ , where  $q_{\parallel} = 2k \sin(\theta)$  and  $k$  is the wavevector of light. Two scattering geometries were studied: the Damon–Eshbach (DE) for spin waves with wavevector  $k$  perpendicular to the external field  $H$ , and the Backward (BA) mode configuration for spin waves with wavevector paralleling to the applied field. Secondly, the angle of incidence of the illuminating laser in this case was fixed at  $\theta = 20^\circ$ . The external field  $H$  was however varied from +4 kOe to  $-4 \text{ kOe}$  and applied along the  $0^\circ$  and  $45^\circ$  orientations with respect to ASI lattices.

Spin-wave dispersions were measured to indicate the possible inter-island dynamic coupling and propagation of collective spin waves through the array. Panels (a) and (b) of figure 2 are shown for the two different magnetic field orientations. Spectra are recorded in the DE configuration for a 3 kOe magnetic field aligned at  $0^\circ$  and  $45^\circ$  angle with respect to the horizontal-group elements of the ASI lattices. When the field is applied at  $45^\circ$ , there are three well-defined peaks in the spectra, while for  $0^\circ$  up to seven peaks are visible in two different frequency ranges with the larger in-plane

wavevector. Frequencies measured for wavenumbers between 0 and  $2 \times 10^7 \text{ m}^{-1}$  are shown in figures 2(c) and (d) with the field applied along an array edge and diagonal orientation. In figure 2(c) the dispersion curve is almost flat. This means the inter-island coupling is negligible in ASI system with this spacing. Another possibility as to why the square ASI would not produce bands with the DE geometry is because that edge modes would be excited for elements parallel to the applied field.

In parts (a) and (b) of figure 3, we show BLS spectra of BA scattering geometry as a function of the incident angle of light  $\theta$  for the different field orientation. In this case, only two modes are clearly visible with a diagonally magnetic field and four spin-wave modes appear while applying a horizontal field with respect to one family of ASI islands. Compared with the DE modes, the modes are close together in frequency for the  $45^\circ$  orientation and spread apart by several GHz for the  $0^\circ$  case. In terms of the dispersion, figures 3(c) and (d) shows that all modes at both parallel field and diagonal field have no significant dispersion, thus excluding any magnonic dynamic inter-island coupling effects.

In recent work, Iacocca *et al* [24] have theoretically calculated the magnonic band structure of square ASI array, and shown that the Brillouin-zone energy variations of band



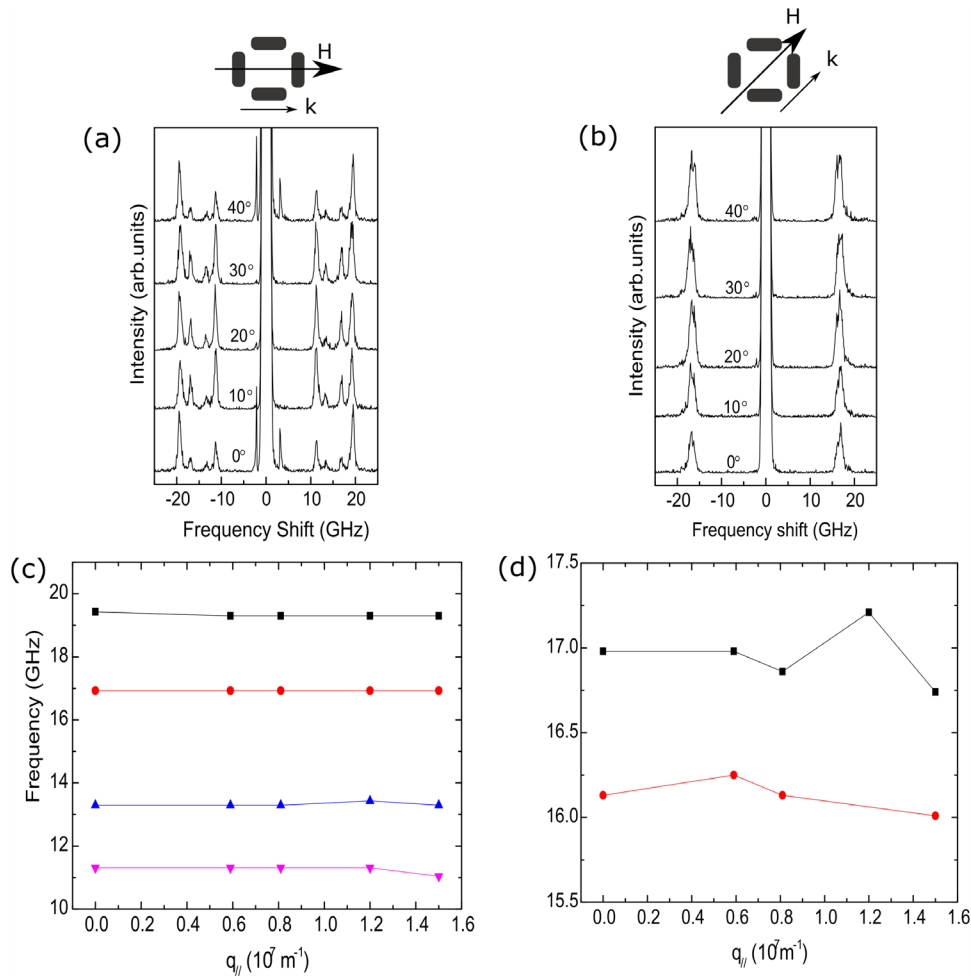


**Figure 3.** Sequence of BLS spectra measured at different incidence angles  $\theta$  with the external field of 3 kOe applied at (a)  $0^\circ$  and (b)  $45^\circ$  external field at 3 kOe with respect to the ASI lattices. The wavevector of the incident light parallels to the applied field in backward configuration. Spin-wave frequency on the Stokes side as a function of the in-plane wavenumber at a 3 kOe (c) horizontal field and (d) diagonal field with respect to the ASI lattice. Dots are the experimental result and lines are guides for the eyes.

structure are in the order of  $10^{-1}$  GHz for spacing similar to our system. This reveals that the inter-element coupling dominated by dipolar interaction in ASI array is very weak, but it still reveals the dispersion behaviour. However, this is below the resolution ability, 0.2–0.4 GHz of BLS technique. Therefore, we can assert that the dynamic inter-element coupling is negligible.

Summaries of the field-induced frequencies are obtained in the DE scattering configuration and presented in figures 4(a) and 5(a). In figure 4(a), the measured frequencies are shown by square symbols, and the magnetic field is oriented along the  $0^\circ$  direction. Several distinct modes are identified from the spectra, and each exhibits different behaviour for fields in the region of hysteresis between  $+4$  and  $-4$  kOe. The frequencies were recorded from spectra obtained by decreasing the field from positive to negative saturation, thereby following the upper branch of the magnetization loop shown in figure 1(a). The behaviour of the frequencies is roughly linear with field outside this region, as one expects for saturated elements.

At the coercive fields, several modes appear to merge with others or disappear entirely. The two lowest frequency modes have minima near the coercive fields. At zero field,

mode crossings appear in two higher frequency modes. These modes in the horizontal islands appear to be softening at negative applied fields. Except for the mode crossings, the behaviour of the mode frequencies for the vertical islands with applied field are symmetrical so that minima again appear for the lowest frequency modes at around  $\pm 1.3$  kOe field marked by two black dashed lines, and there is a linear increase of frequencies for fields outside the hysteresis region.

An analysis of the mode structure was performed using micromagnetic simulations. Using the same parameters as before, dynamics was simulated using Mumax3 following the approach of Vansteenkiste *et al* [25]. The field configuration is shown in figures 1(b) and (d), and again only single elements are considered. The dimensionless damping parameter was set as 0.02, and gyromagnetic ratio  $\gamma = 2.8 \text{ GHz kOe}^{-1}$  was used which was determined from a separate ferromagnetic resonance (FMR) measurement (not shown here) and fitted by a Kittel function [30]. An external field is applied as before, and varied from  $+4$  kOe to  $-4$  kOe.

The frequencies were calculated in the following way. At each field step after relaxation to a steady state configuration a field pulse  $H_e = I_0 \times \frac{\sin(t)}{t} \times \frac{\sin(\Delta ky)}{(\Delta ky)}$  is applied and oriented

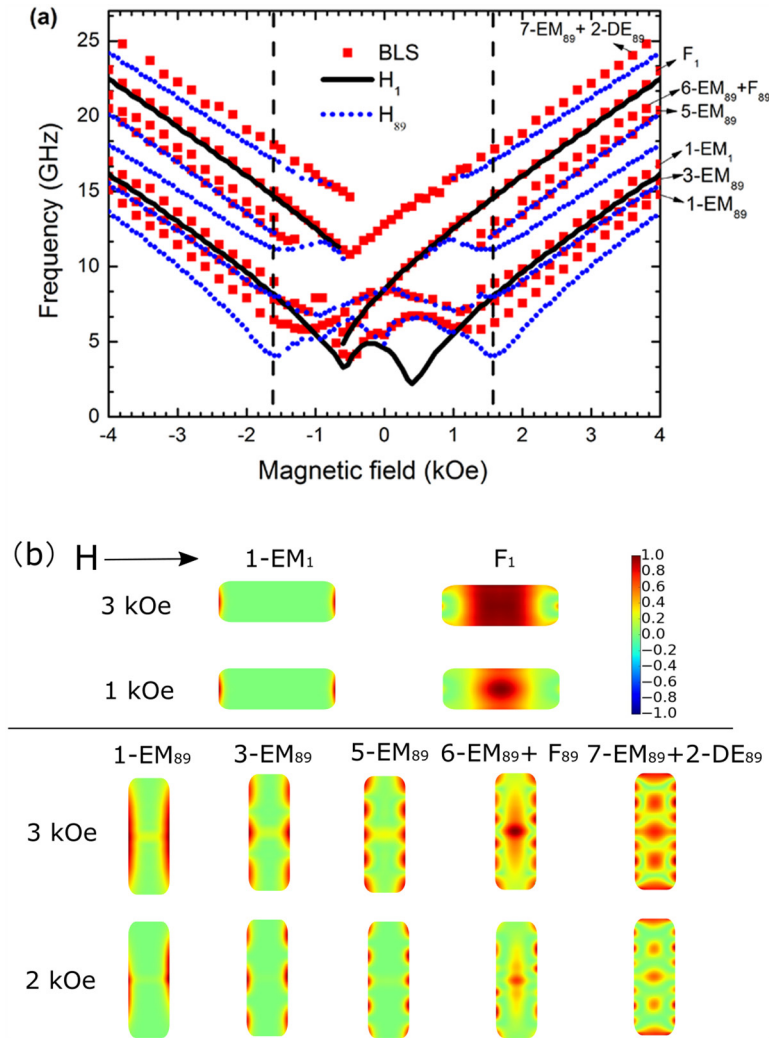


**Figure 4.** (a) Frequencies of the spin-wave eigenmodes as a function of applied field aligned parallel to one group of ASI islands. Dashed lines are the cut-off points between saturated and unsaturated regions of the hard-axis magnetization. (b) Spatial profiles of the eigenmodes at different field strengths for the  $H_1$  (upper panel) and  $H_{89}$  (lower panel) orientations, with frequency increasing from left to right.

along the  $z$  axis. This is expected to lead to torques on each component  $m_x$ ,  $m_y$  and  $m_z$  in each micromagnetic discretization cell, and their responses are recorded every picosecond. Frequencies and intensities of spin-wave modes are then calculated using a discrete Fourier transform (in the time and space) of the magnetisation component,  $m_z$  for each cell [31].

The frequencies calculated in this way are shown in figure 4(a) by the solid lines for  $H_1$  horizontal elements (for which the applied field is collinear) and the dotted blue lines for the  $H_{89}$  vertical elements (for which the applied field is perpendicular to the element axes). Taken together, these simulations describe well the measured frequencies. The small discrepancies may be due in part to the effects of edge roughness [32]. Saturation field can be quite large on the order of several hundred Oe.

To identify which of the confined modes are responsible for the spectra, the spatial profile of the magnetization dynamics  $m_z$  was calculated, and examples are shown in figure 4(b). For the analysis which follows, we use the same classification protocol as in [33]. The modes are classified into four categories: backward ( $m$ -BA), Damon-Eshbach ( $m$ -DE), edge

( $m$ -EM) and fundamental (F). In this classification, the integer  $m$  indicates the number of nodal lines. The BA mode is a mode with a nodal line perpendicular to the magnetization. Nodal lines parallel to the magnetization are called  $m$ -DE. The edge modes,  $m$ -EM, are localised at the ends of the islands and normally have a small intensity in the BLS spectrum. The fundamental F is the Kittel uniform resonance ( $m = 0$ ). This mode typically has the largest intensity.

The modes associated with the horizontal elements are labelled in figure 4(a) as  $1 - EM_1$  and  $F_1$ , representing respectively the EM and fundamental modes. These mode profiles remain unchanged in intensity for magnetic fields between 3 kOe to 1 kOe. The  $F_1$  appears to soften for fields more negative than  $-50$  kOe, consistent with reversal of the magnetization of the horizontal element. We note that the calculated  $1 - EM_1$  mode have two minima in the unsaturated region. This corresponds to curling of the edge magnetization. Note also the difference in amplitude of the F mode for the 1 and 3 kOe fields.

Modes for the vertical elements are labelled  $7 - EM_{89} + 2 - DE_{89}$ ,  $6 - E_{89}M + F_{89}$ ,  $5 - EM_{89}$ ,  $3 - EM_{89}$

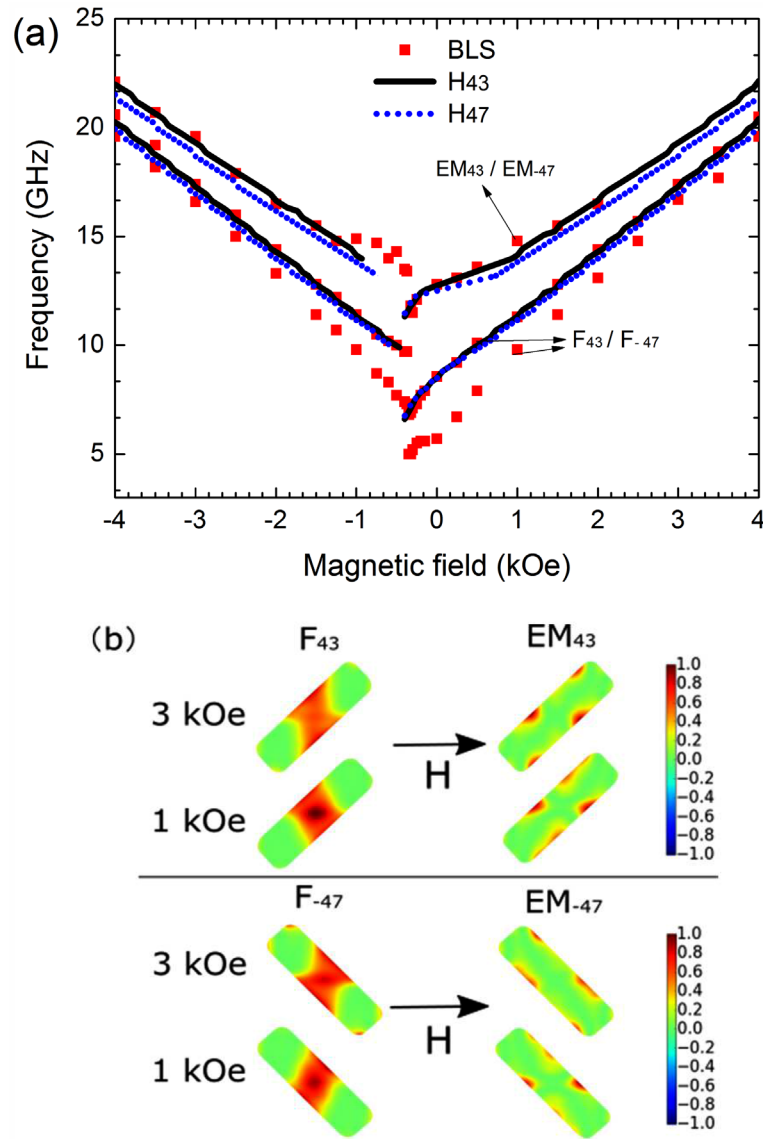


**Figure 5.** (a) Frequencies of the spin-wave modes versus applied field  $H$  with  $45^\circ$  angle with respect to the islands. (b) Spatial profiles of  $m_z$  component magnetization dynamics at (upper panel)  $43^\circ$  and (lower panel)  $-47^\circ$  field angles.

and  $1 - EM_{89}$  in figure 4(a). The corresponding spatial profiles shown in the bottom of the figure 4(b). The  $1 - EM_{89}$  mode is type EM, and possesses the lowest frequency. In the  $5 - EM_{89}$  and  $3 - EM_{89}$  mode the standing wave also emerges. Hybridization is more apparent in the higher frequency modes, a mix of a F mode and a 6-EM mode and a mix with the 7-EM and 2-DE modes. As for the horizontal elements, there is significant dependence of the mode amplitudes on field as seen by comparing the profiles for 2 and 3 kOe. Furthermore, the frequency of the EM mode is smallest at 1.5 kOe as the magnetization begins to saturate perpendicular to the element axis [34].

Spectra and profiles for the case when the external field is aligned diagonally along  $45^\circ$  with respect to ASI edges are shown in figure 5. Hysteresis appears in the modes as a gap at about  $-37$  kOe, corresponding to reversal of the magnetization. In this symmetrical configuration, the modes appear the same for all islands and the two observed modes are F and

EM modes. The spatial profiles of the F mode and EM mode are displayed in figure 5(b). There are subtle changes in the position of the amplitudes for the EM mode when the field is reversed from 3 to 1 kOe. Likewise, the shape of the F mode amplitude changes slightly as the field is reduced, and an edge mode contribution just visible at the corners disappears.

#### 4. Conclusions

In this work, we have investigated the magnetic properties and normal modes of the square ASI using the AGFM and BLS techniques. The square ASI geometry allows for comparisons between modes in elements with orthogonal alignment. The configuration in which the magnetic field is perpendicular to one set of elements (the ‘vertical’ elements in our geometry) reveals complex spectra due to the presence of many types of edge modes. The main features of the modes can be well described as arising from independent elements aligned parallel



and perpendicular to the applied field. We note that although there is no evidence of interactions between elements associated with dynamic fields, the static fields produced by neighbouring elements should be strong enough to produce small shifts in frequencies and may contribute to discrepancies between simulated and observed frequencies. For magnetic elements in the saturated field, the shifts associated with the dynamic inter-element dipolar coupling could not be detected, and would in any case be much smaller from possible contributions of edge defects or other imperfections of the magnetic elements in addition to the static shifts described above. Nevertheless, we have shown that this ASI acts as a reconfigurable microwave resonator and that the exact spectrum observed depends on the microconfiguration of elements in the array.

## Acknowledgments

The work of YL and RLS was supported by the China Scholarship Council and EPSRC (grant number EP/L002922/1), and the work of SAM and CHM in the University of Leeds was also funded by EPSRC (grant number EP/L00285X/1) and supported by Diamond Light Source and Rutherford Appleton Laboratory. We would like to acknowledge that the results of micromagnetic simulation presented here made use of the Emerald High Performance Computing facility made available by the Centre for Innovation. The Centre is formed by the universities of Oxford, Southampton, Bristol, and University College London in partnership with the STFC Rutherford-Appleton Laboratory. The data underpinning this paper are available at <http://dx.doi.org/10.5525/gla.researchdata.358>

## References

- [1] Heyderman L J and Stamps R L 2013 *J. Phys.: Condens. Matter* **25** 363201
- [2] Wang R F *et al* 2006 *Nature* **439** 303
- [3] Kapaklis V *et al* 2012 *New J. Phys.* **14** 035009
- [4] Mengotti E, Heyderman L J, Rodríguez A F, Nolting F, Hügli R V and Braun H-B 2011 *Nat. Phys.* **7** 68
- [5] Bhat V S, Sklenar J, Farmer B, Woods J, Hastings J T, Lee S J, Ketterson J B and De Long L E 2013 *Phys. Rev. Lett.* **111** 077201
- [6] Chern G-W, Morrison M J and Nisoli C 2013 *Phys. Rev. Lett.* **111** 177201
- [7] Gilbert I, Chern G-W, Zhang S, O'Brien L, Fore B, Nisoli C and Schiffer P 2014 *Nat. Phys.* **10** 670
- [8] Zhou X, Chua G-L, Singh N and Adeyeye A O 2016 *Adv. Funct. Mater.* **26** 1437
- [9] Ribeiro I R B, Felix J F, Figueiredo L C, Morais P C, Ferreira S O, Moura-Melo W A, Pereira A R, Quindeau A and de Araujo C I L 2016 *J. Phys.: Condens. Matter* **28** 456002
- [10] Jungfleisch M B *et al* 2016 *Phys. Rev. B* **93** 100401
- [11] Gilbert I, Lao Y, Carrasquillo I, O'Brien L, Watts J D, Manno M, Leighton C, Scholl A, Nisoli C and Schiffer P 2016 *Nat. Phys.* **12** 162
- [12] Rodrigues J H, Mól L A S, Moura-Melo W A and Pereira A R 2013 *Appl. Phys. Lett.* **103** 092403
- [13] Morgan J P, Stein A, Langridge S and Marrows C H 2011 *Nat. Phys.* **7** 75
- [14] Farhan A, Kleibert A, Derlet P M, Anghinolfi L, Balan A, Chopdekar R V, Wyss M, Gliga S, Nolting F and Heyderman L J 2014 *Phys. Rev. B* **89** 214405
- [15] Nisoli C, Wang R, Li J, McConville W F, Lammert P E, Schiffer P and Crespi V H 2007 *Phys. Rev. Lett.* **98** 217203
- [16] Li J, Ke X, Zhang S, Garand D, Nisoli C, Lammert P, Crespi V H and Schiffer P 2010 *Phys. Rev. B* **81** 092406
- [17] Mathieu C *et al* 1997 *Appl. Phys. Lett.* **70** 2912
- [18] Hillebrands B, Mathieu C, Bauer M, Demokritov S O, Bartenlian B, Chappert C, Decanini D, Rousseaux F and Carcenac F 1997 *J. Appl. Phys.* **81** 4993
- [19] Stoecklein W, Parkin S S P and Scott J C 1988 *Phys. Rev. B* **38** 6847
- [20] Hamrle J, Gaier O, Min S-G, Hillebrands B, Sakuraba Y and Ando Y 2009 *J. Phys. D: Appl. Phys.* **42** 084005
- [21] Gubbiotti G, Albin L, Carlotti G, De Crescenzi M, Di Fabrizio E, Gerardino A, Donzelli O, Nizzoli F, Koo H and Gomez R D 2000 *J. Appl. Phys.* **87** 5633
- [22] Gubbiotti G, Conti M, Carlotti G, Candeloro P, Di Fabrizio E, Guslienko K Y, Andre A, Bayer C and Slavin A N 2004 *J. Phys.: Condens. Matter* **16** 7709
- [23] Bayer C *et al* 2005 *Phys. Rev. B* **72** 064427
- [24] Iacocca E, Gliga S, Stamps R L and Heinonen O 2016 *Phys. Rev. B* **93** 134420
- [25] Vansteenkiste A, Leliaert J, Dvornik M, Helsen M, Garcia-Sanchez F and Waeyenberge B V 2014 *AIP Adv.* **4** 107133
- [26] Smith N, Markham D and LaTourette D 1989 *J. Appl. Phys.* **65** 4362
- [27] Youssef J B, Vukadinovic N, Billet D and Labrune M 2004 *Phys. Rev. B* **69** 174402
- [28] Kohli K K, Balk A L, Li J, Zhang S, Gilbert I, Lammert P E, Crespi V H, Schiffer P and Samarth N 2011 *Phys. Rev. B* **84** 180412
- [29] Carlotti G and Gubbiotti G 1999 *Riv. Nuovo Cimento* **22** 1
- [30] Kittel C 1948 *Phys. Rev.* **73** 155
- [31] McMichael R D and Stiles M D 2005 *J. Appl. Phys.* **97** 10J901
- [32] Gubbiotti G, Tacchi S, Carlotti G, Vavassori P, Singh N, Goolaup S, Adeyeye A O, Stashkevich A and Kostylev M 2005 *Phys. Rev. B* **72** 224413
- [33] Gubbiotti G *et al* 2014 *Phys. Rev. B* **90** 024419
- [34] Montoncello F, Giovannini L, Nizzoli F, Vavassori P, Grimsditch M, Ono T, Gubbiotti G, Tacchi S and Carlotti G 2007 *Phys. Rev. B* **76** 024426